Simulation and Modeling of Common Mode EMI Noise in Planar Transformers

LI Wei[1], JI Jingkang[1], LIU Yuanlong[1], SUN Jiawei[2], LIN Subin[2]
(1. ZTE Corporation, Shenzhen 518057, China;
2. Fuzhou University, Fuzhou 350108, China)

DOI: 10.12142/ZTECOM.202303014
https://kns.cnki.net/kcms/detail/34.1294.TN.20230810.1409.004.html, published online August 10, 2023
Manuscript received: 2022-11-21

Abstract: The transformer is the key circuit component of the common-mode noise current when an isolated converter is working. The high-frequency characteristics of the transformer have an important influence on the common-mode noise of the converter. Traditionally, the measurement method is used for transformer modeling, and a single lumped device is used to establish the transformer model, which cannot be predicted in the transformer design stage. Based on the transformer common-mode noise transmission mechanism, this paper derives the transformer common-mode equivalent capacitance under ideal conditions. According to the principle of experimental measurement of the network analyzer, the electromagnetic field finite element simulation software three-dimensional (3D) modeling and simulation method is used to obtain the two-port parameters of the transformer, extract the high-frequency parameters of the transformer, and establish its electromagnetic compatibility equivalent circuit model. Finally, an experimental prototype is used to verify the correctness of the model by comparing the experimental measurement results with the simulation prediction results.

Keywords: planar transformer; electromagnetic compatibility; common-mode noise; simulation; modeling

Citation (Format 1): LI W, JI J K, LIU Y L, et al. Simulation and modeling of common mode EMI noise in planar transformers [J]. ZTE Communications, 2023, 21(3): 105 - 116. DOI: 10.12142/ZTECOM.202303014
Citation (Format 2): W. Li, J. K. Ji, Y. L. Liu, et al., "Simulation and modeling of common mode EMI noise in planar transformers," *ZTE Communications*, vol. 21, no. 3, pp. 105 - 116, Jun. 2023. doi: 10.12142/ZTECOM.202303014.

1 Introduction

Isolated power converters are widely used in applications that require isolation between the input side and the output side. However, due to the high voltage and current rate of change when switching devices in the power converter are turned on or off, serious electromagnetic interference (EMI) noise is generated[1]. For converters including isolation transformers, the critical path of common-mode noise includes the distributed capacitance between the primary and secondary windings of the transformer in addition to the direct-to-ground coupling capacitance of the voltage trip point[2-4]. The transmission mechanism of common mode noise and the establishment of an electromagnetic compatibility model are of great significance for the analysis and suppression of common mode noise of isolated power converters.

Magnetic components in power converters often occupy a large volume. As power converters develop toward high power density, traditional wound transformers are gradually replaced by planar transformers due to their disadvantages of large size and weight. Planar transformers generally use multi-layer printed circuit board (PCB) traces as windings. The primary and secondary windings are tightly coupled, with low leakage inductance. At the same time, the core height is greatly reduced, so that planar transformers have a smaller size, which is widely used in isolated converters with high power density[5-7]. However, the copper thickness of the printed circuit board is limited by the process. In order to improve the current capacity, it is necessary to increase the width of the planar transformer windings and adopt the method of multi-layer parallel wiring, which will greatly increase the facing area between the primary and secondary windings of the planar transformer, increase the distributed capacitance between the windings, and deteriorate the high-frequency characteristics of the planar transformer[8]. For the integrally installed planar transformer, its printed circuit board windings and the main circuit share the same PCB, and its discrete devices cannot be obtained to evaluate its electromagnetic compatibility characteristics. Therefore, the relevant parameters of the electromagnetic compatibility equivalent circuit model of the planar transformer can be extracted through electromagnetic field simulation software. Compared with the traditional wound transformer, the structural parameters of the planar transformer are stable and consistent, and it is easy to model in the electromagnetic field finite element simulation software.

In Ref. [9], considering the winding potential gradient distribution of planar transformers, a two-capacitance model based on common-mode current equivalence is derived based on the winding structure theory. However, the results obtained from the theoretical calculation consider the common-mode equivalent capacitance to be constant, ignoring the case that the common-mode equivalent capacitance is no longer a pure capacitance at high frequencies. Refs. [10 – 11] propose a method for evaluating the common-mode EMI characteristics of transformers using vector network analyzer experimental measurements. In this method, the transformer is treated as a common-mode noise filter, and the insertion loss parameter S_{21} [12 – 13] used to evaluate the EMI filter performance is referenced into the transformer. The experiment proves that it is feasible and effective to use the insertion loss measurement principle to evaluate the common mode noise rejection capability of the transformer. However, Refs. [10 – 11] only use S_{21} as the evaluation basis without further analyzing the specific meaning of the complete S-parameters obtained by the vector network analyzer to measure the transformer.

Section 2 analyzes the common mode noise transmission mechanism of the planar transformer, and deduces the expression of the induced charge Q between the primary and secondary windings according to the potential distribution of the windings when the planar transformer is working. From the expression, two capacitors are sufficient to represent the common-mode noise of the transformer. Section 3 establishes the electromagnetic compatibility equivalent circuit model of planar transformers according to the common mode noise transmission mechanism and the energy transmission characteristics of the transformer and introduces a method to establish the electromagnetic compatibility model of the full-bridge transformer through the experimental measurement of the network analyzer. Section 4 is based on the principle of experimental measurement and modeling of the network analyzer, and the two-port parameters of the planar transformer are extracted through the electromagnetic field finite element simulation software without physical objects, and are equivalent to a circuit model. Finally, the accuracy of the simulation modeling is verified by a full-bridge circuit prototype experiment in Section 5. Section 6 concludes this paper.

2 Transmission Mechanism of Common Mode Noise in Planar Transformers

2.1 Structural Capacitance Calculation

The common-mode noise transmission of the planar transformer is mainly through the distributed capacitance between the primary winding and the secondary winding. It is worth noting that the distributed capacitance of the transformer is not equal to the equivalent capacitance of the common mode noise, because the voltage on the planar transformer winding is not a constant value. However, the derivation of the common-mode noise equivalent capacitance is based on the distributed capacitance of the planar transformer. The simulation results of a one-turn-to-one-turn circular plane copper wire are shown in Fig. 1. Fig. 1(a) shows a simulation model of a one-turn-to-one-turn circular planar copper conductor. In Fig. 1(c), the planar transformer winding uses PCB wiring, and the distance d between the turns of the primary and secondary windings is the distance between the layers of the PCB. For a planar transformer with a single-layer single-turn structure, considering the current flow factor, the wiring width w of the winding is generally much larger than d, and the distributed capacitance between the primary winding and the secondary winding can be approximately regarded as a parallel plate capacitor, ignoring the edge effect. Then the structural capacitance C_0 between turns in Fig. 1(c) can be expressed as:

$$C_0 = \frac{\varepsilon_r \varepsilon_0 S}{d}, \tag{1}$$

where ε_r is the dielectric constant of the filling material between the PCB layers, ε_0 is the dielectric constant in vacuum, S is the facing area between turns, and d is the distance between turns.

Since the method of approximating parallel plate capacitors is used in the calculation of the capacitance of the planar transformer structure, in order to test the rationality and accuracy of the approximation, the electromagnetic field finite element simulation software is used to verify the winding structural capacitance.

Taking a turn-to-turn ring-shaped flat copper wire as an example, we list the model parameters as follows: the copper thickness is 1 mm, the inner diameter is 12.3 mm, the outer

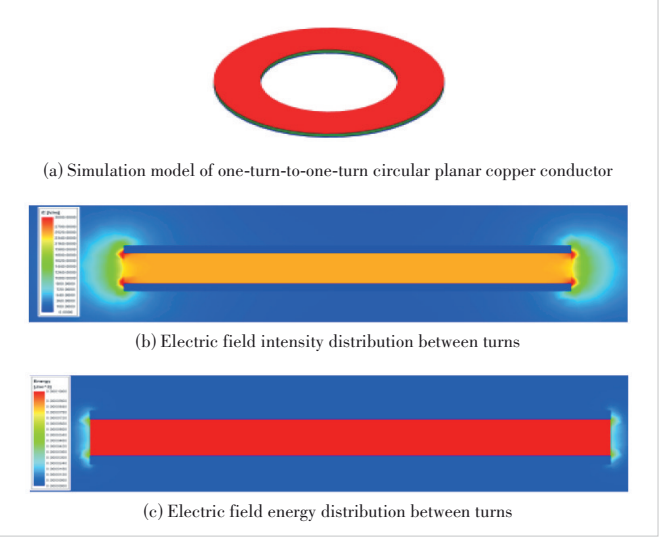

(a) Simulation model of one-turn-to-one-turn circular planar copper conductor

(b) Electric field intensity distribution between turns

(c) Electric field energy distribution between turns

▲ **Figure 1. Simulation results of one-turn-to-one-turn toroidal planar copper conductors**

diameter is 20.6 mm, the distance between turns is 0.4 mm, and the relative permittivity of the filler material is 4.4.

The simulation result of the finite element simulation software is 21.769 pF, and the calculation result of Eq. (1) is 20.89 pF, with an error of 4.04%. The main source of error is the edge effect of the parallel plate capacitor. In Fig. 1(b), the electric field strength between conductors is basically uniform, and the electric field distribution at the edge of the conductor is obviously uneven. However, Fig. 1(c) shows that most of the electric field energy is stored between conductors, so it is reasonable to use an approach that approximates a parallel plate capacitor.

2.2 Calculation of Equivalent Capacitance for Common Mode Noise of Planar Transformers

For a planar transformer, due to the close magnetic coupling of each layer of windings, the magnetic flux or induced electromotive force linked by each turn of the winding is basically the same, and the alternating current (AC) resistance of each turn of the winding is much smaller than the excitation inductance. If the leakage inductance is ignored, it can be approximated that the potential of the winding is linearly distributed along the number of turns and the length of the winding.

Assuming that the potential on the transformer winding in Fig. 1(a) is linearly distributed along the turn length, and the distributed capacitance is evenly distributed along the winding, the integral of the primary winding and the secondary winding along the turn length l can be expressed as:

$$\int_0^l v_{\mathrm{p}}(x)\mathrm{d}x = \frac{v_{\mathrm{ph}} + v_{\mathrm{pl}}}{2} \cdot l, \tag{2}$$

$$\int_0^l v_{\mathrm{s}}(x)\mathrm{d}x = \frac{v_{\mathrm{sh}} + v_{\mathrm{sl}}}{2} \cdot l. \tag{3}$$

The charge Q stored between the turns of the primary and secondary windings in Fig. 1(a) can be expressed as:

$$Q = \int_0^l \frac{C_0}{l} \cdot \left[v_{\mathrm{p}}(x) - v_{\mathrm{s}}(x)\right]\mathrm{d}x = \frac{C_0}{l}\left[\int_0^l v_{\mathrm{p}}(x)\mathrm{d}x - \int_0^l v_{\mathrm{s}}(x)\mathrm{d}x\right]. \tag{4}$$

Substituting Eqs. (2) and (3) into Eq. (4), we can get:

$$Q = C_0\left(\frac{v_{\mathrm{ph}} + v_{\mathrm{pl}}}{2} - \frac{v_{\mathrm{sh}} + v_{\mathrm{sl}}}{2}\right). \tag{5}$$

Considering that when the windings between different turns of the planar transformer are connected, the outlet ports of the windings on the same side need to be staggered by a certain angle. At this time, the voltage difference between the relative position of the primary winding and the secondary winding will change with the staggered angle. However, it can be obtained from Eq. (5) that the induced charge Q between turns is determined by the structural capacitance C_0 between the primary and secondary windings and the midpoint potential of the primary and secondary windings. As long as the assumption of uniform distribution of potential on the windings is established, the charge Q is not affected by the voltage difference distribution of the primary and secondary windings. As long as the assumption of uniform distribution of potential on the windings holds, the charge Q is not affected by the voltage difference distribution of the primary and secondary windings. As shown in Fig. 2, the angles between the primary winding outlet port and the secondary winding outlet port are 180°, 135° and −135°. The potential difference between the primary winding and the secondary winding changes. However, ignoring the influence of port voids, after the integration operation of Eq. (4), the final induced charge Q between turns and the turns of three different outlet port angles is the same.

The primary and secondary windings of a planar transformer are multi-turn, so it is only necessary to follow the calculation method of Eq. (5). The inductive charge between each turn of the primary and secondary windings is added up to the charge Q_{all} stored between the primary and secondary windings of the entire planar transformer. Q_{all} characterizes the transfer capability of transformer common mode noise.

Taking the single-layer single-turn planar transformer in Fig. 3 as an example to calculate Q_{all}, we find that the turn ratio of the primary and secondary windings is 3:1, the primary winding has 3 turns, which are P_1, P_2, and P_3, respectively, and the secondary winding has 1 turn, which is S_1. The transformer adopts a 2-layer parallel winding on the primary side, an 8-layer parallel winding on the secondary side, and a staggered winding on the primary and secondary sides. The specific stacked structure is shown in Fig. 3. At the same time, the laminated structure parameters of the planar transformer are given in Table 1. Under the symmetrical structure, the facing areas between P_1, P_2, P_3 and S_1 are basically the same, and S is uniformly taken as the facing area between the turns of the primary and secondary windings.

The charge $Q_{P_1S_1}$ stored between the first turn P_1 of the primary winding and the secondary winding S_1 can be expressed as:

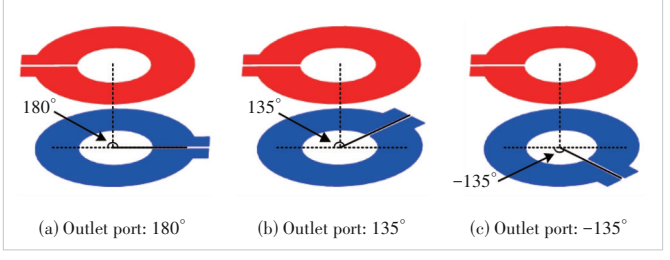

▲**Figure 2. Schematic diagrams of different angles of the outlet ports of the primary and secondary windings**

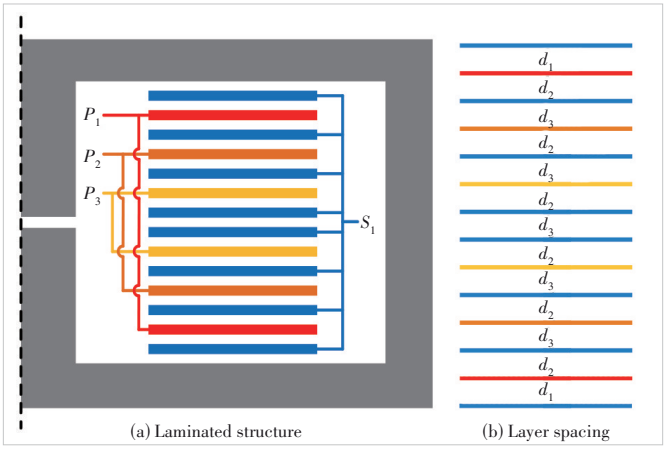

▲ **Figure 3. Schematic diagram of the laminated structure of a planar transformer**

▼**Table 1. Planar transformer laminated structure parameters**

d_1/mil	d_2/mil	d_3/mil	S/mm^2
4.5	4.3	5	214.5

$$Q_{p_1s_1} = C_{p_1s_1}(v_{p_1m} - v_{s_1m}), \tag{6}$$

where $C_{p_1s_1}$ is the total structural capacitance between P_1 and S_1, v_{p_1m} is the midpoint voltage of P_1, and v_{s_1m} is the midpoint voltage of S_1.

In the same way, the charge $Q_{P_2S_1}$ stored between the second turn P_2 of the primary winding and the secondary winding S_1 is:

$$Q_{p_2s_1} = C_{p_2s_1}(v_{p_2m} - v_{s_1m}), \tag{7}$$

where $C_{p_2s_1}$ is the total structural capacitance between P_2 and S_1, and v_{p_2m} is the midpoint voltage of P_2.

The charge $Q_{P_3S_1}$ stored between the third turn P_3 of the primary winding and the secondary winding S_1 is:

$$Q_{p_3s_1} = C_{p_3s_1}(v_{p_3m} - v_{s_1m}), \tag{8}$$

where $C_{p_3s_1}$ is the total structural capacitance between P_3 and S_1, and v_{p_3m} is the midpoint voltage of P_3.

Then the charge Q_{all} stored between the primary and secondary windings of the entire planar transformer can be expressed as:

$$Q_{\text{all}} = Q_{p_1s_1} + Q_{p_2s_2} + Q_{p_3s_3}, \tag{9}$$

From the perspective of the entire planar transformer, the planar transformer in Fig. 4 has four endpoints: A, B, C, and D, where A and C are ends with the same name. According to the relationship between the voltage ratio of the primary and secondary sides of the transformer and the turn ratio, it can be known that the voltage drop Δv_p per turn of the primary winding of the transformer is the same as the voltage drop Δv_s per turn of the secondary winding. If the voltage drop per turn is Δv, then we have:

$$\Delta v = \frac{v_p}{N_p} = \frac{v_s}{N_S}, \tag{10}$$

where v_p is the port voltage of the entire primary winding of the planar transformer, v_s is the port voltage of the entire secondary winding of the planar transformer, N_p is the number of turns of the primary winding of the planar transformer, and N_s is the number of turns of the secondary winding of the planar transformer. According to the stacked structure of the planar transformer, N_p takes 3 and N_s takes 1.

Considering the voltage distribution of the planar transformer winding in Fig. 4, it is only necessary to select the voltage of a certain point on the primary winding of the transformer as the voltage reference point, and the potential of any other point can be expressed by the voltage reference point and the voltage drop Δv per turn; the same is true for the secondary winding.

The point inside the transformer winding is used as the voltage reference point. When modeling, the model of the transformer needs to be split, which complicates the modeling. Therefore, in order to simplify the modeling, the four terminals A, B, C, and D of the transformer are used as alternative voltage reference points. By selecting point B of the primary winding and point D of the secondary winding as the potential reference points, the midpoint potentials v_{p_1m}, v_{p_2m}, v_{p_3m} and v_{S_1m} of each turn winding in the planar transformer can be expressed as:

$$v_{p_1m} = v_B + 2.5\Delta v, \tag{11}$$

$$v_{p_2m} = v_B + 1.5\Delta v, \tag{12}$$

$$v_{p_3m} = v_B + 0.5\Delta v, \tag{13}$$

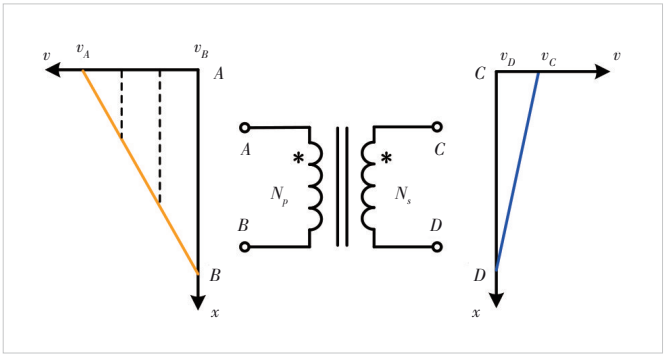

▲ **Figure 4. Flat transformer winding voltage distribution**

$$v_{s_1 m} = v_D + 0.5\Delta v\,. \tag{14}$$

Substituting Eqs. (6) – (8) and Eqs. (11) – (14) into Eq. (9), the total induced charge Q_{all} can be expressed as:

$$Q_{\text{all}} = \left(C_{p_1 s_1} + C_{p_2 s_1} + C_{p_3 s_1}\right) v_{\text{BD}} + \left(2C_{p_1 s_1} + C_{p_2 s_1}\right)\Delta v, \tag{15}$$

where $C_{p_1 s_1}$, $C_{p_2 s_1}$, and $C_{p_3 s_1}$ are quantitative after the planar transformer structure and material are determined, and the induced charge Q_{all} can be calculated with only two voltage variables v_{BD} and Δv. Q_{all} reflects the induced charge between the primary and secondary windings, and replaces the voltage variable Δv with the voltage variables v_{AD} and v_{BD} between the primary and secondary windings, as shown in Eq. (16).

$$\Delta v = \frac{v_A - v_B}{3} = \frac{v_{AD} - v_{BD}}{3}. \tag{16}$$

Substituting Eq. (16) into Eq. (15) and eliminating Δv, we can get:

$$Q_{\text{all}} = \left(\frac{1}{3}C_{p_1 s_1} + \frac{2}{3}C_{p_2 s_1} + C_{p_3 s_1}\right) v_{BD} + \left(\frac{2}{3}C_{p_1 s_1} + \frac{1}{3}C_{p_2 s_1}\right) v_{AD}. \tag{17}$$

Eq. (17) shows that the induced charge Q_{all} is divided into two parts, and the induced charge Q_{all} can be reduced to the transformer port BD and port AD. Then the expressions of capacitance C_{BD} and C_{AD} are:

$$C_{BD} = \frac{1}{3}C_{p_1 s_1} + \frac{2}{3}C_{p_2 s_1} + C_{p_3 s_1}, \tag{18}$$

$$C_{AD} = \frac{2}{3}C_{p_1 s_1} + \frac{1}{3}C_{p_2 s_1}\,. \tag{19}$$

The capacitance C_{BD} between B and D and the capacitance C_{AD} between A and D are the equivalent common-mode capacitance of the planar transformer. The sum of the induced charges at both ends of the capacitance C_{BD} and C_{AD} is Q_{all}. The corresponding two-capacitor models of the transformer are shown in Fig. 5.

3 Electromagnetic Compatibility Equivalent Circuit Model of Planar Transformer

The electromagnetic compatibility equivalent circuit model of the full-bridge transformer is shown in Fig. 6. This model can not only realize the energy transmission characteristics of the transformer but also reflect its electromagnetic compatibility characteristics.

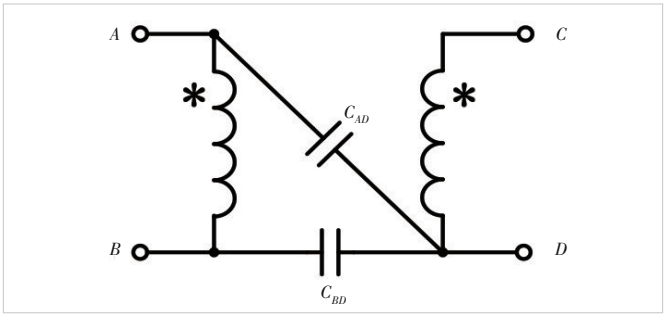

▲Figure 5. Two-capacitor model

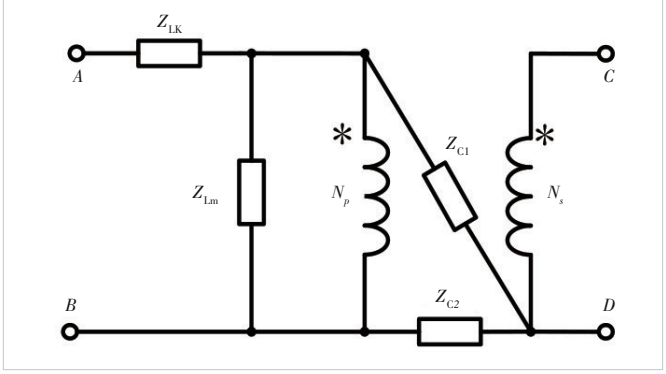

▲Figure 6. Electromagnetic compatibility equivalent circuit model of planar transformer

N_p represents the number of turns of the primary winding, N_s the number of turns of the secondary winding, Z_{Lk} the leakage inductance impedance, Z_{Lm} the magnetizing inductance impedance, and Z_{C1} and Z_{C2} the common mode equivalent capacitance impedance. When the frequency is low, Z_{Lk} and Z_{Lm} can be represented by pure inductance, and Z_{C1} and Z_{C2} can be represented by pure capacitance. However, as the frequency increases, the electromagnetic environment inside the transformer becomes more and more complex, and the electromagnetic compatibility characteristics inside the transformer can no longer be represented by the pure inductance or pure capacitance model of these four impedance parameters. At the same time, in order to take into account the basic circuit functions of transmitting energy, the lumped concept is adopted, and the positions of Z_{Lk}, Z_{Lm}, Z_{C1}, and Z_{C2} are kept unchanged. According to the specific impedance curve of the four parameters, a high-order model composed of inductance, resistance and capacitance is used to represent the electromagnetic compatibility equivalent circuit model of the planar transformer. At the operating frequency of the switch tube of the isolated converter, the model can realize the energy transfer from the primary side to the secondary side, and at the frequency of conducted electromagnetic interference, the model can reflect the electromagnetic compatibility characteristics of the transformer.

To extract Z_{C1} and Z_{C2}, it is necessary to simulate the actual working conditions of the planar transformer in the full-bridge circuit, and to form the same potential distribution on

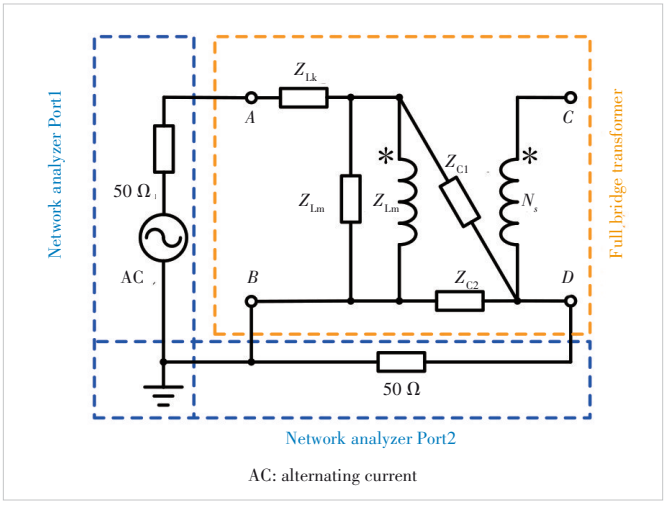

▲ **Figure 7. Schematic diagram of the simulation wiring diagram of the actual working condition of the full-bridge transformer**

the primary and secondary windings of the transformer as the actual working condition. Fig. 7 shows the schematic diagram of the simulation wiring diagram of the actual working condition of the full-bridge transformer. The network analyzer Port1 applies voltage excitation. The excitation output terminal of Port1 is connected to the primary winding point *A* of the full-bridge transformer, and the other excitation output reference terminal is connected to the primary winding point *B* of the full-bridge transformer. The network analyzer Port2 receives the common mode noise current generated by the planar transformer, the signal-receiving terminal of Port2 is connected to the secondary winding point *D*, and the other signal-receiving reference terminal is connected to the primary winding point *B*.

The measurement result of the network analyzer is the scattering matrix, that is, the *S*-parameter matrix, which describes the relationship between the reflected wave of the port voltage and the incident wave. According to the relationship between the port voltage and the current, the *S*-parameter matrix can be converted into a *Z*-parameter matrix, as shown in Eq. (20).

$$\begin{cases} Z_{11} = Z_0 \dfrac{(1+S_{11})(1-S_{22}) + S_{12}S_{21}}{(1-S_{11})(1-S_{22}) - S_{12}S_{21}} \\ Z_{12} = Z_0 \dfrac{2S_{12}}{(1-S_{11})(1-S_{22}) - S_{12}S_{21}} \\ Z_{21} = Z_0 \dfrac{2S_{21}}{(1-S_{11})(1-S_{22}) - S_{12}S_{21}} \\ Z_{22} = Z_0 \dfrac{(1-S_{11})(1+S_{22}) + S_{12}S_{21}}{(1-S_{11})(1-S_{22}) - S_{12}S_{21}} \end{cases}, \quad (20)$$

where S_{21} and S_{12} are the transmission coefficients in the scattering matrix, S_{11} and S_{22} are the reflection coefficients in the scattering matrix, and Z_0 is the characteristic impedance.

According to the test principle, the magnetic field of the magnetic core of the planar transformer is excited during the test, the potential distribution of the primary and secondary windings of the transformer is formed, and the leakage magnetic field between the primary and secondary windings is formed. Therefore, the network analyzer measures a two-port network containing transformer leakage inductance Lk, excitation inductor Lm, and equivalent common-mode capacitors C1 and C2. We simplify the wiring schematic of Fig. 7 and obtain an equivalent circuit diagram for measurement as shown in Fig. 8.

According to the circuit theory, the two-port *Z*-parameter can be expressed as:

$$\begin{cases} \dot{U}_1 = Z_{11}\dot{I}_1 + Z_{12}\dot{I}_2 \\ \dot{U}_2 = Z_{21}\dot{I}_1 + Z_{22}\dot{I}_2 \end{cases}. \quad (21)$$

The test result of the network analyzer is a two-port matrix, which makes Fig. 8 further equivalent to the two-port network of Fig. 9, and the *Z*-parameter expression of the two ports is shown in Eq. (21). For the reciprocal two-port network with three variables Z_{11}, $Z_{12}(=Z_{21})$, and Z_{22}, three equations can be listed, and three unknowns can be solved theoretically.

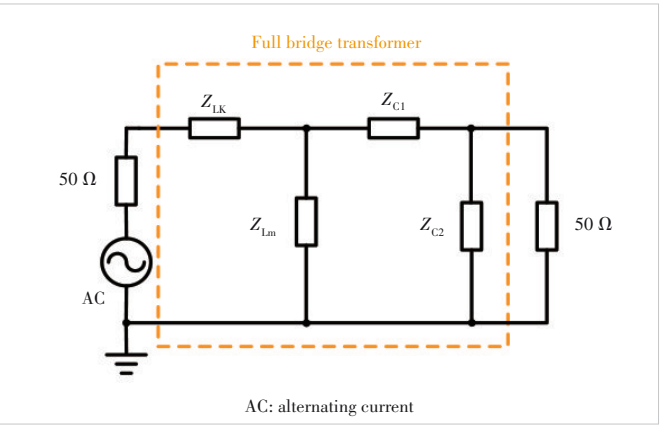

▲ **Figure 8. Equivalent circuit diagram of simulated wiring of full-bridge transformer in actual working conditions**

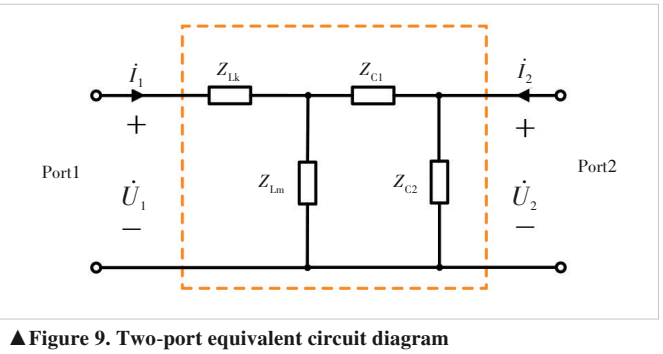

▲ **Figure 9. Two-port equivalent circuit diagram**

Therefore, for the above two-port equivalent circuit, first, the transformer secondary port *CD* in Fig. 6 is short-circuited, and the leakage inductance impedance Z_{Lk} is measured using a network analyzer or impedance analyzer. In Fig. 9, given Z_{Lk}, opening the port Port2, we can get Eqs. (22) and (23):

$$Z_{11} = \frac{\dot{U}_1}{\dot{I}_1}\bigg|_{\dot{I}_2 = 0} = Z_{Lk} + Z_{Lm} // \left(Z_{C1} + Z_{C2}\right), \tag{22}$$

$$Z_{12} = Z_{21} = \frac{\dot{U}_2}{\dot{I}_1}\bigg|_{\dot{I}_2 = 0} = \frac{\left[Z_{Lm} // \left(Z_{C1} + Z_{C2}\right)\right] Z_{C2}}{Z_{C1} + Z_{C2}}. \tag{23}$$

By opening Port1, Z_{22} can be represented as:

$$Z_{22} = \frac{\dot{U}_2}{\dot{I}_2}\bigg|_{\dot{I}_1 = 0} = Z_{C2} // \left(Z_{C1} + Z_{Lm}\right). \tag{24}$$

Combining Eqs. (22) – (24), we can get the expressions of Z_{Lm}, Z_{C1} and Z_{C2} with Z_{Lk}, and Z_{11}, Z_{12} and Z_{22} as variables:

$$Z_{Lm} = \frac{Z_{11}Z_{22} - Z_{21}^{\ 2} - Z_{Lk}Z_{22}}{Z_{22} - Z_{21}}, \tag{25}$$

$$Z_{C1} = \frac{Z_{11}Z_{22} - Z_{21}^{\ 2} - Z_{Lk}Z_{22}}{Z_{21}}, \tag{26}$$

$$Z_{C2} = \frac{Z_{11}Z_{22} - Z_{21}^{\ 2} - Z_{Lk}Z_{22}}{Z_{11} - Z_{Lk} - Z_{21}}. \tag{27}$$

Z_{Lm}, Z_{C1} and Z_{C2} can be solved according to Eqs. (25) – (27). After obtaining the impedance curves of the parameters Z_{Lm}, Z_{C1}, Z_{C2} and Z_{Lk} required for modeling, the circuit parameters of the electromagnetic compatibility equivalent circuit model of the planar transformer are determined by the method of circuit model fitting.

4 Planar Transformer Simulation

4.1 Extraction of Material Parameters of Planar Transformer Core

To obtain the impedance curves of magnetic core materials such as inductors and transformers with the help of simulation tools, it is first necessary to extract the complex permeability of the magnetic core material. The complex permeability of the magnetic core material has an important influence on the electromagnetic compatibility characteristics of magnetic components, and is of great significance for the product design selection of magnetic components and the research on electromagnetic compatibility characteristics. Although the data sheets provided by some magnetic core material manufacturers will include the complex permeability of the magnetic core material, the complex permeability frequency range provided in the data sheet is usually in the range of several kHz to several MHz, which cannot completely cover the frequency band range of conducted electromagnetic interference research (150 kHz – 30 MHz). Therefore, it is necessary to extract the complex permeability of the magnetic core material through experimental measurement.

Because the distribution parameters of magnetic components are very rich, there are distributed capacitances between the magnetic core and the windings, and between the windings. To reduce the effect of distributed capacitance on complex permeability measurements, the complex permeability of a magnetic core is measured using a single-turn centering method, as shown in Fig. 10. The single-turn winding uses copper wires with a short length and a major diameter to reduce the influence of the winding loss and lead inductance of the single-turn winding on the measurement of the complex magnetic permeability of the magnetic core.

The impedance characteristic of the single-turn coil is measured with an impedance analyzer. The equivalent model of the measurement is:

$$Z = R_s + j\omega L_s, \tag{28}$$

where R_s and L_s are the equivalent series resistance and equivalent series inductance of the magnetic component under test, respectively. It can be approximated that the R_s in the test result is only generated by the core loss, and L_s is only generated by the magnetic permeability of the magnetic core.

Thus according to the definition of complex permeability:

$$\mu = \mu' - j\mu'', \tag{29}$$

▲ **Figure 10. Experimental diagram of the single-turn through-center measurement method**

where μ' is the real permeability and μ'' is the imaginary permeability. The equivalent series model of the core impedance can be expressed as:

$$Z = j\omega \frac{\mu N^2 A_e}{l_e}, \tag{30}$$

where N is the number of turns of the winding, l_e is the equivalent magnetic circuit length, A_e is the cross-sectional area of the magnetic core, and ω is the measured angular frequency.

Substituting Eq. (29) into Eq. (30), we can get:

$$Z = j\omega \frac{(\mu' - j\mu'')N^2 A_e}{l_e}. \tag{31}$$

Comparing Eqs. (28) and (31), we can get the real and imaginary parts of the complex permeability of the magnetic core as follows:

$$\mu' = \frac{L_s l_e}{N^2 A_e}, \tag{32}$$

$$\mu'' = \frac{R_s l_e}{\omega N^2 A_e}. \tag{33}$$

The core loss tangent is:

$$\tan(\theta) = \frac{\mu''}{\mu'}. \tag{34}$$

In order to verify that the complex permeability obtained by the experimental measurement can truly represent the core parameters of the actual sample in the finite element simulation software, an impedance analyzer is used to extract the complex permeability of the magnetic ring in Fig. 11 according to the method in Fig. 10. The impedance analyzer

▲Figure 11. Actual core samples

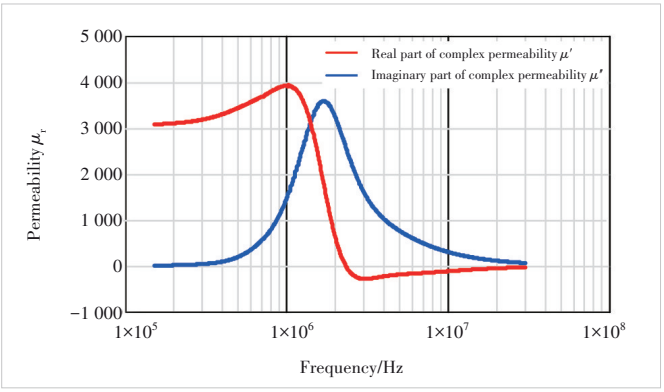

▲Figure 12. Real and imaginary parts of core complex permeability extracted by the impedance analyzer

model is WK 6500B, the core material of the magnetic ring is DMR96, the measured outer diameter is 25 mm, the inner diameter is 15 mm, and the height is 7 mm.

The real and imaginary parts of the complex magnetic permeability of the magnetic ring obtained by the impedance analyzer are shown in Fig. 12.

4.2 Planar Transformer Simulation Modeling

The measurement of the two-port parameters of the planar transformer by the network analyzer is introduced previously. According to the measurement results, the impedance curves of the leakage inductance, magnetizing inductance and equivalent common mode capacitance of the transformer are obtained, and the electromagnetic compatibility equivalent circuit model of the transformer is established. However, the method based on the actual sample measurement of the transformer cannot realize the prediction of conducted EMI noise in the design stage of planar transformer, and the method of deriving the equivalent capacitance of common-mode noise based on the theory of transformer winding stacked structure can only reflect the transmission characteristics of transformer common-mode noise at low frequency. The electromagnetic field finite element simulation software HFSS of Ansys can simulate the function of the network analyzer, obtain the two-port Z-parameters of the transformer, and realize the extraction of the wide-band parameters of the planar transformer without physical objects. At the same time, due to the use of a planar transformer, the accuracy and consistency of the winding structure parameters are higher than those of the traditional manual winding transformer, which is conducive to improving the consistency between the simulation model and the real thing.

Take the planar transformer of the full-bridge circuit as an example. The magnetizing inductance is designed to be 110 μH, the turn ratio of the primary winding and the secondary winding is 3:1, the number of turns on the primary side is 3, and the number of turns on the secondary side is 1. The core material is DMR96, the relative permittivity of

plate FR4 is set to 4.4, and the physical diagram and simulation model of the planar transformer are shown in Fig. 13. The physical diagram of Fig. 13(a) shows that the planar transformer of the full-bridge circuit is integrally installed. We import the PCB of the full-bridge circuit into the simulation software and separate the PCB layout of the winding part of the planar transformer to establish the simulation model of the planar transformer.

The actual planar transformer magnetic core is composed of two magnetic cores. Generally, in order to control the inductance of the magnetizing inductance during the production process, an air gap will be opened on the central column of the magnetic core. This air gap is very small and difficult to measure accurately, but the size of the air gap can be determined by comparing the magnetizing inductance. In the simulation, the transformer's secondary winding is left open and the primary winding is excited, and the input impedance curve can be obtained, which includes the magnetizing inductance, the leakage inductance and the inter-turn capacitance of the transformer. Since the planar transformer adopts the interleaved winding method, the leakage inductance is far smaller than the magnetizing inductance. The input impedance curve at a low frequency can be approximately regarded as the impedance curve of the magnetizing inductance. After determining the size of the air gap, we short-circuit the secondary winding to obtain the leakage inductance Z_{Lk} impedance curve of the transformer. After that, we add excitation according to the measurement method in Fig. 7 to obtain the Z-parameter impedance curve of the transformer at two ports, and derive Z_{Lm}, Z_{C1}, and Z_{C2} in the model according to Eqs. (25) – (27). The simulation results are shown in Fig. 14.

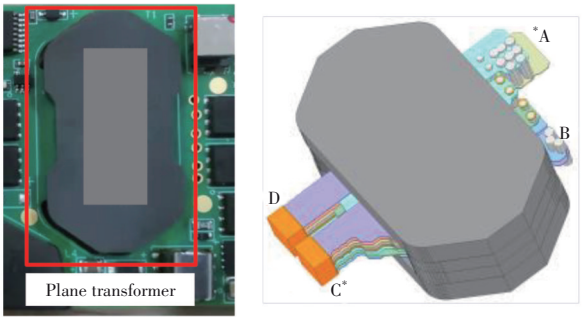

(a) Full bridge circuit plane transformer

(b) Simulation model of planar transformer

▲Figure 13. Full-bridge circuit planar transformer simulation model

5 Experimental Verification

We use the full-bridge circuit module in the wireless base station power supply as the experimental prototype. The rated input voltage of the full-bridge circuit module is 48 V, the rated output voltage is 12 V, the rated output current is 35.8 A, and the operating frequency of the circuit is 170 kHz. The experimental prototype is shown in Fig. 15. The planar transformer used in the experimental prototype is the transformer mentioned above. The conduction test of the full bridge circuit is shown in Fig. 15.

According to the generation and conduction mechanism of common mode noise which is mainly caused by the instantaneous potential change when the switching device is turned on or off, and the distributed capacitance that exists between the power supply and ground is affected by the rising and falling edges of the switching device voltage, resulting in noise currents flowing through the line impedance stabilization network (LISN), ground, and P and N lines with the same amplitude and direction. The common-mode noise cir-

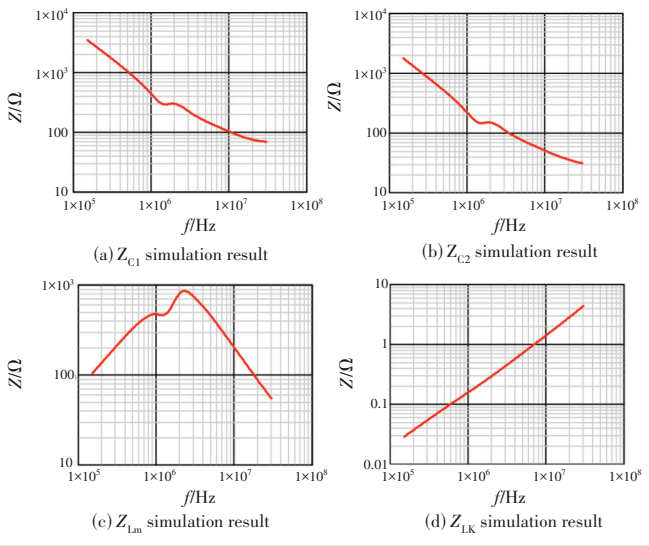

(a) Z_{C1} simulation result

(b) Z_{C2} simulation result

(c) Z_{Lm} simulation result

(d) Z_{LK} simulation result

▲Figure 14. Planar transformer simulation results

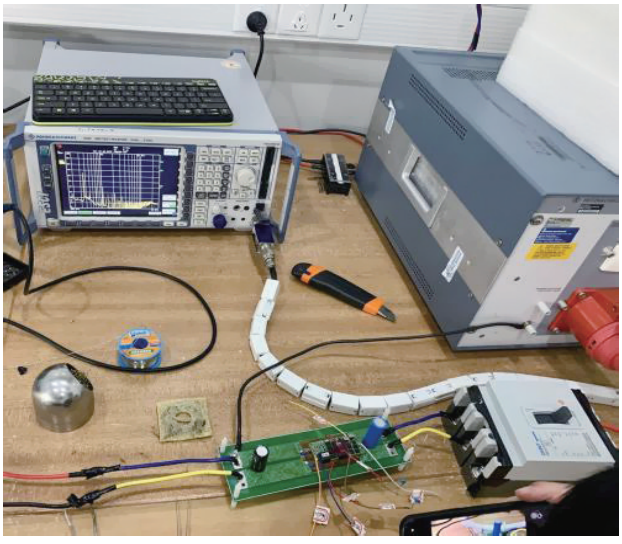

▲Figure 15. Full bridge circuit conduction test

cuit of the full-bridge circuit is shown in Fig. 16. There are 5 main potential jump points, of which the four potential jump points are the 4 terminals of the transformer. Part of the common-mode noise current at the two potential trip points on the primary side of the transformer conducts the common-mode noise current to ground through the switching device's coupling capacitor to the ground, and the other part of the common-mode noise current is transmitted from the primary side to the secondary side through the interturn capacitance of the transformer through the potential change of the transformer primary side and the secondary side winding, and then flows into the earth, LISN, and back to the primary side. For the two potential jump points on the secondary side of the transformer, since the secondary side is connected to the ground, the common-mode noise current flowing through the coupling capacitor between the switching device and ground flows directly back on the secondary side without flowing through the LISN.

According to the substitution theorem, the switches Q_1, Q_3, Q_6, and Q_7 and the output inductor L_o are equivalent to current sources, and the switches Q_2, Q_4, Q_5, and Q_8 are equivalent to voltage sources. The input capacitor C_{in} and the output capacitor C_o can be regarded as a short circuit due to their small impedance, and the common mode impedance Z_{cm} of the LISN can be regarded as 25 Ω. The equivalent circuit diagram after the application of the substitution theorem is shown in Fig. 17.

When the current sources work together, all voltage sources are short-circuited, and an equivalent circuit diagram can be obtained. The primary current source is short-circuited, the voltage at the transformer port is 0, and the secondary side current source is connected in parallel across the secondary winding of the transformer, which is also short-circuited. All current sources are short-circuited when the current source is active, and no common mode noise current is formed in Zcm. The equivalent circuit diagram considering only the current source is shown in Fig. 18.

When the voltage sources work together, open all current sources to obtain the equivalent circuit diagram. The equivalent circuit diagram considering only the voltage sources is shown in Fig. 19. Q_2, Q_4 and Q_8 will generate common mode noise current on Z_{cm}. Using the superposition theorem for the voltage sources Q_2, Q_4, and Q_8, the common-mode noise voltage $\dot{V}_{cm}$ generated on Z_{cm} can be found:

$$\dot{V}_{cm}=\frac{-1}{\left(\frac{1}{Z_{cm}}+\frac{1}{Z_{AD}}+\frac{1}{Z_{BD}}\right)-\frac{1}{Z_{AD}}\cdot\frac{\frac{1}{Z_{AD}}}{\frac{1}{Z_{Lk}}+\frac{1}{Z_{Lm}}+\frac{1}{Z_{AD}}}}\cdot\left[\frac{1}{Z_{Lm}}\cdot\dot{V}_{Q_8}+\frac{1}{Z_{BD}}\cdot\dot{V}_{Q_4}+\frac{1}{Z_{AD}}\cdot\left(\frac{\frac{1}{Z_{Lk}}\cdot\dot{V}_{Q_2}+\frac{1}{Z_{Lm}}\dot{V}_{Q_4}}{\frac{1}{Z_{Lk}}+\frac{1}{Z_{Lm}}+\frac{1}{Z_{AD}}}\right)\right]+\dot{V}_{Q_8}. \quad (35)$$

We use an oscilloscope to measure the voltage waveforms $\dot{V}_{Q_2}$, $\dot{V}_{Q_4}$, and $\dot{V}_{Q_8}$ across the switching tubes Q_2, Q_4, and Q_8, perform Fourier decomposition on them, substitute the results into Eq. (35) to obtain the predicted noise spectrum, and compare it with the measured results, which is shown in

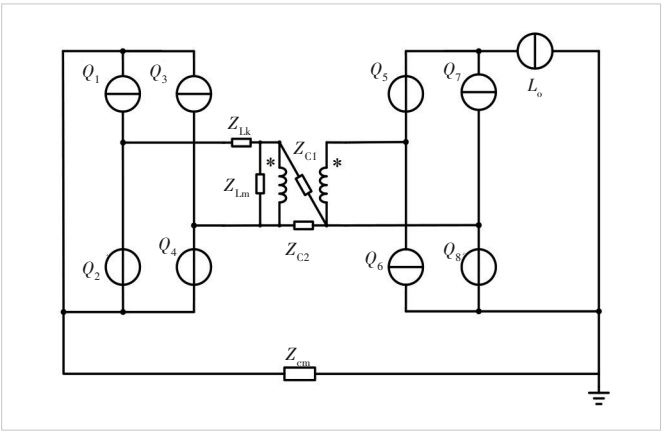

▲Figure 17. Equivalent circuit diagram after applying the substitution theorem

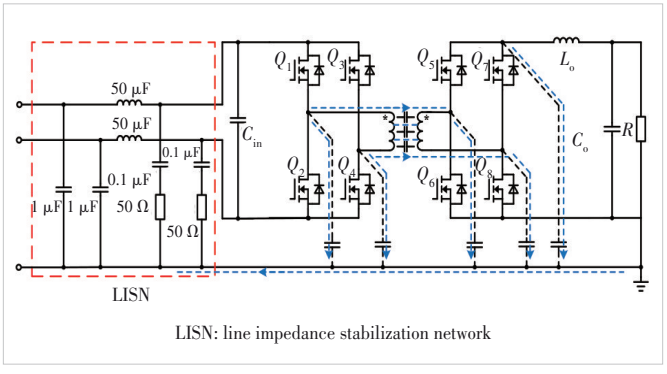

▲Figure 16. Full-bridge circuit noise path

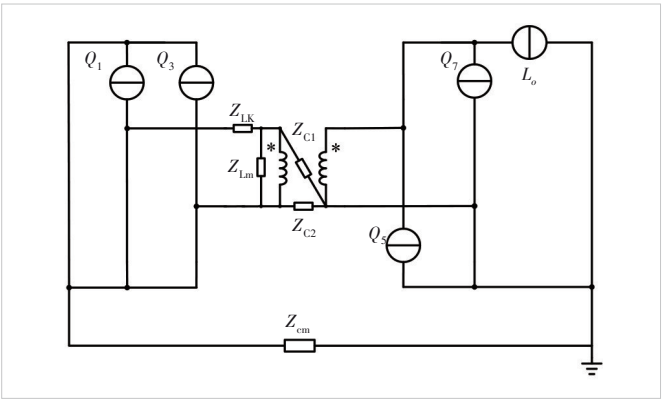

▲Figure 18. Equivalent circuit diagram considering only current source

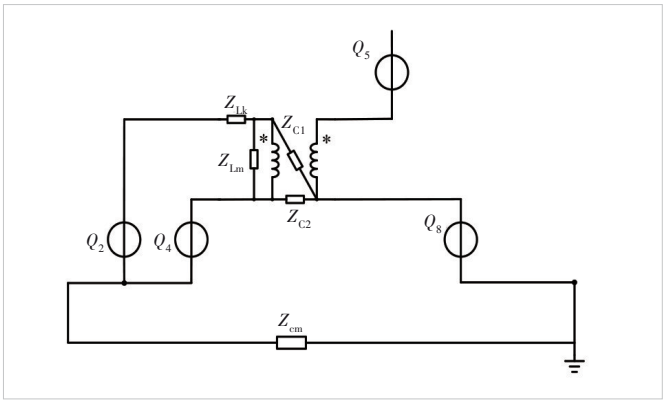

▲Figure 19. Equivalent circuit diagram considering only the voltage source

Fig. 20. The noise prediction results are in good agreement with the measured results, which shows the accuracy of the extraction and modeling of the common mode noise equivalent circuit of the planar transformer.

6 Conclusions

In this paper, the mechanism of common-mode noise conduction of planar transformers is analyzed and a method for extracting planar transformer models through simulation is introduced. The following conclusions are obtained:

1) The common-mode noise transmission capability of planar transformers is reflected in the induced charge Q between the primary and secondary windings of planar transformers. At the same time, according to the theoretical derivation of the potential distribution on the planar transformer winding, the induced charge Q can be represented by two capacitors.

2) When using a network analyzer to measure a planar transformer, the measurement result is a two-port network including leakage inductance, magnetizing inductance, and inter-turn capacitance.

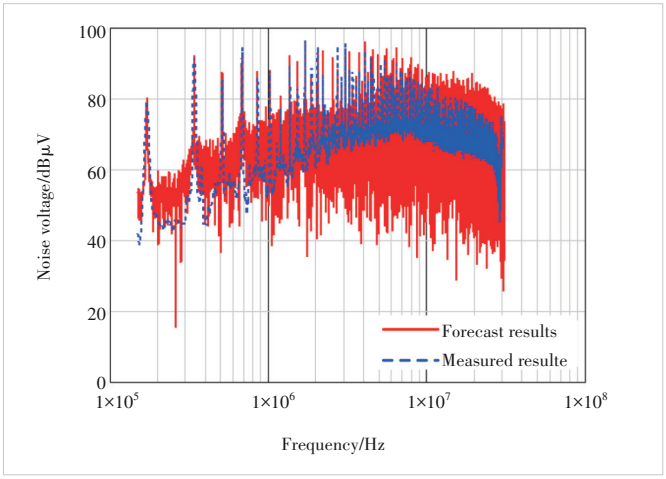

▲Figure 20. Predicted noise spectrum and measured noise spectrum

3) With the help of the simulation software, the Z-parameters of the planar transformer can be obtained, and the EMI model of the planar transformer can be established through the Z-parameters. Finally, the accuracy of the simulation and modeling is verified through a full-bridge circuit prototype experiment.

References

[1] MOHAMMADI M, ADIB E, YAZDANI M R. Family of soft-switching single-switch PWM converters with lossless passive snubber [J]. IEEE transactions on industrial electronics, 2015, 62(6): 3473 - 3481. DOI: 10.1109/TIE.2014.2371436
[2] LI Y M, ZHANG H, WANG S, et al. Investigating switching transformers for common mode EMI reduction to remove common mode EMI filters and Y-capacitors in flyback converters [J]. IEEE journal of emerging and selected topics in power electronics, 2018, 6(4): 2287 - 2301. DOI: 10.1109/JESTPE.2018.2827041
[3] ZHANG H, WANG S, LI Y M, et al. Two-capacitor transformer winding capacitance models for common-mode EMI noise analysis in isolated DC - DC converters [J]. IEEE transactions on power electronics, 2017, 32(11): 8458 - 8469. DOI: 10.1109/TPEL.2017.2650952
[4] CHU Y B, WANG S. A generalized common-mode current cancelation approach for power converters [J]. IEEE transactions on industrial electronics, 2015, 62(7): 4130 - 4140. DOI: 10.1109/TIE.2014.2387335
[5] TRIA L A R, ZHANG D M, FLETCHER J E. Planar PCB transformer model for circuit simulation [J]. IEEE transactions on magnetics, 2016, 52(7): 1 - 4. DOI: 10.1109/tmag.2016.2516995
[6] ALI SAKET M, ORDONEZ M, SHAFIEI N. Planar transformers with near-zero common-mode noise for flyback and forward converters [J]. IEEE transactions on power electronics, 2018, 33(2): 1554 - 1571. DOI: 10.1109/TPEL.2017.2679717
[7] MASWOOD A I, SONG L K. Design aspects of planar and conventional SMPS transformer: A cost benefit analysis [J]. IEEE transactions on industrial electronics, 2003, 50(3): 571 - 577. DOI: 10.1109/TIE.2003.812469
[8] ALI SAKET M, SHAFIEI N, ORDONEZ M. Planar transformer winding technique for reduced capacitance in LLC power converters [C]//Proceedings of 2016 IEEE Energy Conversion Congress and Exposition (ECCE). IEEE, 2017: 1 - 6. DOI: 10.1109/ECCE.2016.7855352
[9] ZHANG Z L, HE B H, HU D D, et al. Common-mode noise modeling and reduction for 1-MHz eGaN multioutput DC - DC converters [J]. IEEE transactions on power electronics, 2019, 34(4): 3239 - 3254. DOI: 10.1109/TPEL.2018.2850351
[10] CHEN Q B, CHEN W. An evaluation method of transformer behaviors on the suppression of common-mode conduction noise in switch mode power supply [J]. Proceedings of the CSEE, 2012, 32(18): 73-79+180
[11] FU K N, CHEN W. Evaluation method of flyback converter behaviors on common-mode noise [J]. IEEE access, 2019, 7: 28019 - 28030. DOI: 10.1109/ACCESS.2019.2902462
[12] LIU S, ZHANG Y T, YU D Y. Research and design of EMI digital filters using scattering parameters [C]//International Conference on Wireless Communications & Signal Processing. IEEE, 2009: 1 - 5. DOI: 10.1109/WCSP.2009.5371392
[13] WANG S, LEE F C, ODENDAAL W G. Characterization and parasitic extraction of EMI filters using scattering parameters [J]. IEEE transactions on power electronics, 2005, 20(2): 502 - 510. DOI: 10.1109/TPEL.2004.842949
[14] FRICKEY D A. Conversions between S, Z, Y, H, ABCD, and T parameters which are valid for complex source and load impedances [J]. IEEE transactions on microwave theory and techniques, 1994, 42(2): 205 - 211. DOI: 10.1109/22.275248

Biographies

LI Wei (li.wei27@zte.com.cn) received his MS degree in mechatronic engineering from Southeast University, China in 2017. Currently he is working as an EMC engineer in ZTE Corporation. His research interests include switching power supply of EMC and lightning protection.

JI Jingkang received his MS degree in mechatronic engineering from Southeast University, China in 2020. He currently works as an EMC engineer in ZTE Corporation. His research interests include switching power supply of EMC and reverberation chambers.

LIU Yuanlong received his MS degree from Harbin Institute of Technology, China. Currently he is working as an EMC engineer in ZTE Corporation. His research interests include lightning protection, switching power supply of EMC, and engineering safety.

SUN Jiawei received his BE degree in electrical engineering and automation and ME degree in power electronics and power transmission both from Fuzhou University, China in 2018 and 2022, respectively. His research interest focuses on power electronics high frequency magnetic technology.

LIN Subin received his doctor's degree from Fuzhou University, China. He currently works as an associate professor with the School of Electrical Automation, Fuzhou University. He has been engaged in the theoretical research and technical development of power electronic magnetic components for a long time. His main research direction is power electronic electromagnetic component technology, electromagnetic compatibility analysis and diagnosis.